J Biol Inorg Chem (2012) 17:27–36
DOI 10.1007/s00775-011-0822-7

ORIGINAL PAPER

Mechanistic insight from thermal activation parameters for oxygenation reactions of different substrates with biomimetic iron porphyrin models for compounds I and II

Christoph Fertinger · Alicja Franke · Rudi van Eldik

Received: 8 April 2011 / Accepted: 7 July 2011 / Published online: 30 July 2011

Abstract Compound I, an oxo–iron(IV) porphyrin π-cation radical species, and its one-electron-reduced form compound II are regarded as key intermediates in reactions catalyzed by cytochrome P450. Although both reactive intermediates can be easily produced from model systems such as iron(III) *meso*-tetra(2,4,6-trimethylphenyl)porphyrin hydroxide by selecting appropriate reaction conditions, there are only a few thermal activation parameters reported for the reactions of compound I analogues, whereas such parameters for the reactions of compound II analogues have not been investigated so far. Our study demonstrates that $\Delta H^{\neq}$ and $\Delta S^{\neq}$ are closely related to the chemical nature of the substrate and the reactive intermediate (viz., compounds I and II) in epoxidation and C–H abstraction reactions. Although most studied reactions appear to be enthalpy-controlled (i.e., $\Delta H^{\neq} > -T\Delta S^{\neq}$), different results were found for C–H abstractions catalyzed by compound I. Whereas the reaction with 9,10-dihydroanthracene as a substrate is also dominated by the activation enthalpy ($\Delta H^{\neq} = 42$ kJ/mol, $\Delta S^{\neq} = 41$ J/Kmol), the same reaction with xanthene shows a large contribution from the activation entropy ($\Delta H^{\neq} = 24$ kJ/mol, $\Delta S^{\neq} = -100$ J/kmol). This is of special interest since the activation barrier for entropy-controlled reactions shows a significant dependence on temperature, which can have an important impact on the relative reaction rates. As a consequence, a close correlation between bond strength and reaction rate—as commonly assumed for C–H abstraction reactions—no longer exists. In this way, this study can contribute to a proper evaluation of experimental and computational data, and to a deeper understanding of mechanistic aspects that account for differences in the reactivity of compounds I and II.

Keywords Iron porphyrin · Enzyme models · Activation parameters · Peroxide · O–O bond activation

Introduction

The heme-containing cytochromes P450 form a superfamily of enzymes that are ubiquitous in aerobic organisms. High-valence iron(IV)–oxo porphyrin species have been identified as key intermediates in a vast number of reactions catalyzed by these enzymes and their iron porphyrin biomimetics [1–4]. Throughout the past decades, there was a vivid discussion among scientists to clarify the different pathways for oxygenation reactions that lead to different reaction products or product distributions. Computational studies support a two-state reactivity [3–19] of an iron(IV)–oxo porphyrin cation radical with closely lying quartet (high-spin) and doublet (low-spin) states showing different reactivity patterns. In comparison to this theoretical work, our own experimental work [20] ruled out an involvement of an iron(III)–peroxo species, compound 0 [(Por)Fe^{III}-OOR] (Por is porphyrin), as an oxidant in catalytic reactions as proposed in the "multiple oxidant hypothesis" [21–30].

Regardless of this intriguing controversy, it should be kept in mind that even very fundamental effects coming

Electronic supplementary material The online version of this article (doi:10.1007/s00775-011-0822-7) contains supplementary material, which is available to authorized users.

C. Fertinger · A. Franke · R. van Eldik (✉)
Inorganic Chemistry,
Department of Chemistry and Pharmacy,
University of Erlangen-Nuremberg,
Egerlandstrasse 1, 91058 Erlangen, Germany
e-mail: vaneldik@chemie.uni-erlangen.de

from the solvent [22, 26] or the axial ligands [26, 31–35] can have a dramatic impact on the observed reactivity or even change the underlying reaction mechanism. Therefore, in our recent work [36] we clarified the influence of the nature of different substrates on their reaction with different reactive intermediates that can participate in iron porphyrin catalyzed reactions, i.e., compound 0, the iron(IV)–oxo porphyrin cation radical species compound I [(Por$^{\cdot+}$)Fe^{IV}=O], and its one-electron-reduced form compound II [(Por)Fe^{IV}=O]. We demonstrated a close relationship between the chemical nature of a substrate and its reactivity towards different reactive intermediates and also revealed changes in the reactivity order for compounds 0, I, and II by investigating different types of reactions.

Especially changes in the regioselectivity in competitive olefin oxygenation experiments leading to C=C epoxidation and allylic C–H hydroxylation products are still the subject of intense international research [21–26, 31–35]. In this context, special attention was focused on the influence of the *meso* substituents of the porphyrin system [37–40]. Recent studies [41, 42] demonstrated that a simple change in the *meso* substituents can even change the regioselectivity from C=C epoxidation to C–H hydroxylation in the reaction of olefins with the cation radical species compound I. Computational studies revealed that this change in the reaction mechanism is caused by changes in the electronic nature of the porphyrin as well as by interactions of the substrate with the ligand on the *meso* substituents of the porphyrin system that affect the orientation of the substrate towards the iron–oxo center.

Thus, experimental as well as computational studies suggest large effects on the activation barrier of certain types of reactions that can, for example, be accounted for in terms of substrate orientation as mentioned above [43]. In addition, the rates of hydrogen abstraction show a close correlation with the energies of the C–H bonds in question, which obviously should be reflected in the activation barrier of the reaction. To clarify which effect dominates in hydrogen abstraction and epoxidation reactions, we determined the thermal activation parameters $\Delta H^{\neq}$ and $\Delta S^{\neq}$ for the reactions of some selected substrates with model porphyrin complexes for compound I, which is the most crucial intermediate discussed as part of P450 catalysis, and for its one-electron-reduced form compound II. Although compound II is known to be a sluggish oxidant compared with compound I [4], it is still a competent catalyst in a number of different reactions [36]. As this is the first study to investigate enthalpy and entropy effects for compound II, and moreover the first to compare activation parameters for both of the most discussed active species involved in catalytic oxygenation reactions, it provides new insight into mechanistic aspects that influence the reactivity of compounds I and II.

Materials and methods

Materials

All solutions were prepared in acetonitrile (99.9% AMD CHROMASOLV from Sigma-Aldrich) *m*-Chloroperoxybenzoic acid was purchased from Acros Organics and purified before use by recrystallization from hexane. Iron(III) *meso*-tetra(2,4,6-trimethylphenyl)porphyrin hydroxide [Fe^{III}(TMP)OH; Scheme 1] was obtained from iron(III) *meso*-tetra(2,4,6-trimethylphenyl)porphyrin chloride [Fe^{III}(TMP)Cl; Frontier Scientific] as described earlier [44]. The resulting Fe^{III}(TMP)OH was washed thoroughly with water to remove trace impurities of NaOH, which could affect the proper generation of compound I or compound II owing to the pH sensitivity of these reactions. Iodosylbenzene was synthesized according to a literature procedure [45]. 9,10-Dihydroanthracene (DHA), 9*H*-xanthene, and *cis*-stilbene (96%) were purchased from Aldrich (Scheme 2).

Low-temperature rapid-scan measurements

Time-resolved UV/vis spectra were recorded with a quartz glass dip-in detector (Spectralytics, Aalen, Germany) coupled to a J&M TIDAS 500-3 (TSPEC-4) diode-array spectrophotometer (J&M Analytik, Esslingen, Germany). The optical dip-in detector had an optical path length of 1.0 cm and was connected to the spectrophotometer with flexible light guides. A 20 ml double-wall reaction vessel was used and thermostatted (±0.1 °C) by a combination of cold methanol circulation (WK 14-1 DS; Colora, Lorch, Germany) and a 800 W heating unit. Complete spectra were recorded between 350 and 726 nm with the integrated software program J&M TIDAS-DAQ 2.3.7.4.

Results

Iron(III) *meso*-tetramesitylporphyrin complexes are known to be good biomimetics to study the catalytic reactions of cytochrome P450 since the choice of an appropriate oxidant in combination with carefully selected reaction conditions allows a proper generation and sufficient stabilization of different reactive intermediates, i.e., compounds 0, I, and II, in solution for several minutes [20, 36].

The addition of an excess of *m*-chloroperoxybenzoic acid to a solution of [Fe^{III}(TMP)OH] or [Fe^{III}(TMP)Cl] in acetonitrile at low temperatures leads to the formation of the cation radical species [(TMP$^{\cdot+}$)Fe^{IV}=O] (compound I). This is due to an acid-catalyzed heterolytic cleavage of the O–O bond (two-electron oxidation), in which the excess of *m*-chloroperoxybenzoic acid provides the necessary protons [20, 36, 46, 47].

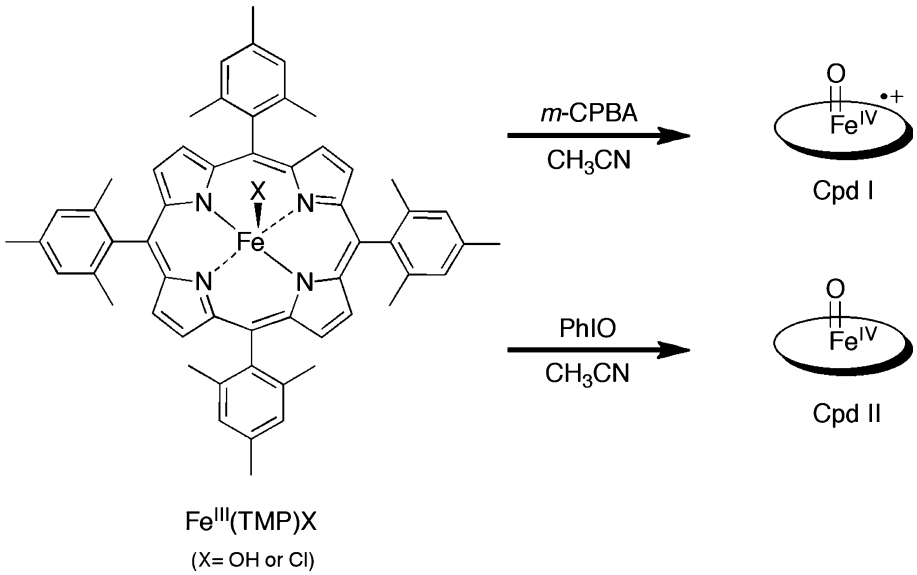

Scheme 1 Structure of Fe^{III}(TMP)X [TMP is *meso*-tetra(2,4,6-trimethylphenyl)porphyrin] and its reaction with *m*-chloroperoxybenzoic acid (*m-CPBA*) or iodosylbenzene (*PhIO*) to produce compound I (*Cpd I*) or compound II (*Cpd II*), respectively

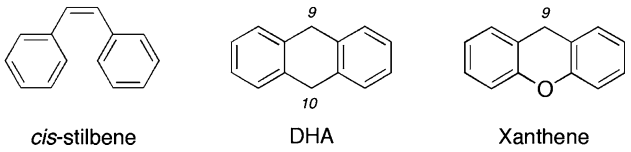

Scheme 2 Structures of the substrates employed, viz., *cis*-stilbene, 9,10-dihydroanthracene (*DHA*), and 9*H*-xanthene

In aprotic solvents such as acetonitrile, the choice of a nonacidic oxidizing agent—in our case iodosylbenzene—converts [Fe^{III}(TMP)OH] into compound II [(TMP)Fe^{IV}=O] (see Scheme 1) [36, 48, 49].

Compounds I and II can be easily identified by careful analysis of the spectral changes observed in the resulting time-resolved UV/vis spectra. The formation of compound I is associated with a large absorbance decrease and a shift to a shorter wavelength of the Soret band combined with an absorbance increase between 550 and 700 nm, which is characteristic for a high-valence oxo–iron(IV) porphyrin π-cation radical, [(TMP$^{\cdot+}$)Fe^{IV}=O] (see Figs. 1, S1) [20, 36].

In contrast to the cation radical compound I, the plain iron(IV)–oxo species compound II shows a small shift to a longer wavelength together with an absorbance increase of the Soret band. Furthermore, a new broad band at 550 nm occurs, which can be used to identify compound II spectroscopically (Figs. 1, S2) [36]. Unlike similar model complexes, [Fe^{III}(TMP)OH] is known to form compound II as the sole stable product under these conditions [36, 49]. We found no evidence for the formation of a mixture of reactive intermediates as reported for other systems [50], i.e., compound II and traces of compound I formed via disproportionation of compound II. In fact, the cation radical band of compound I is absent when compound II is

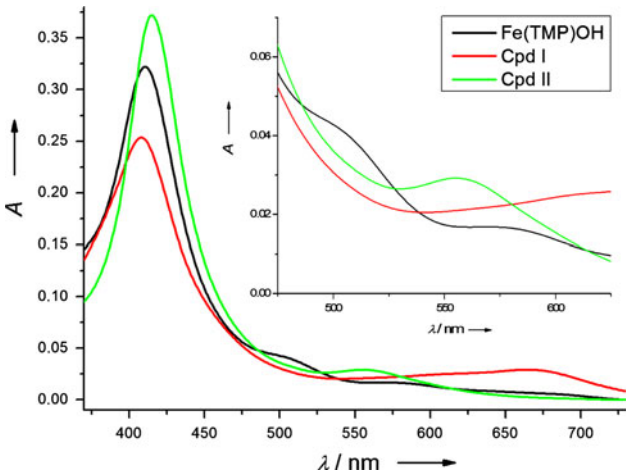

Fig. 1 Comparison of the UV/vis spectra for compound I (*red line*) and compound II (*green line*) produced from [Fe^{III}(TMP)OH] (TMP is *meso*-tetra(2,4,6-trimethylphenyl)porphyrin) (*black line*). *Inset*: Magnified view of the spectra between 475 and 625 nm

formed, and clean isosbestic points as well as clean one-exponential kinetic fits support this observation.

Furthermore, an experiment that is commonly used to prove the existence of a mixture of reactive intermediates [50] was performed. The addition of various amounts of [Fe^{III}(TMP)OH], after the formation of compound II by a minimum amount of iodosylbenzene and prior to the addition of substrate, should suppress the fast disproportionation reaction of compound II and therefore the formation of the very reactive compound I. Under such conditions, the observed rate constants for the oxygenation of the substrate (concentrations of the oxidant and the substrate were kept constant in each experiment) should be inversely proportional to the concentration of added [Fe^{III}(TMP)OH]. However, this experiment revealed only

very small changes (within the experimental error limits) in the resulting rate constants with increasing concentration of added [Fe^{III}(TMP)OH]. This is further strong evidence that compound II is indeed the sole active oxidant in the system studied.

Since compounds I and II can be selectively produced and unambiguously identified by their characteristic UV/vis spectra, temperature-dependent measurements can be performed as these intermediates show a remarkable stability for many minutes in acetonitrile over a sufficiently wide temperature range.

Compounds I and II were produced in solution as described already, and their formation and stability in solution were continuously monitored by UV/vis spectroscopy before the addition of the substrate. In the course of this study, three different substrates were used (see Scheme 2). *cis*-Stilbene is a common substrate used to investigate epoxidation of olefins by compound I or compound II [20, 36, 51, 52], whereas DHA and 9*H*-xanthene were used to study C–H abstraction reactions (see Schemes 3, 4) [36, 52, 53]. The latter are known to be the rate-determining initial steps in dehydrogenation and hydroxylation reactions [10, 41, 43], operating in compliance with the "rebound mechanism," which was initially postulated by Groves et al. [54] more than 30 years ago and which is still gaining growing support by current research [55]. Important to note, there are two possible pathways following the initial C–H abstraction step [41]. In the case of DHA, a dehydrogenation rather than a hydroxylation step is expected to operate, leading to anthracene as a very stable aromatic product [53].

In the same way, epoxidation reactions can be investigated, where the rate-determining step is the initial C–O bond formation (see Scheme 4) [10, 51, 52]. Competing hydroxylation/epoxidation reactions [41] do not play a role when these substrates are used, as on the one hand *cis*-stilbene does not bear any saturated hydrocarbons necessary for C–H abstraction, and on the other hand DHA and xanthene lack double bonds accessible for epoxidation. In general, benzylic hydrogen is known to be a rather sluggish reaction partner in hydroxylation reactions [56], so these possible side reactions have no impact on our studies.

Regardless of the particular oxygenation products, the rate constants determined in dehydrogenation/hydroxylation and epoxidation reaction sequences concern the rate-determining initial reaction steps. These steps are identical for compounds I and II, i.e., hydrogen abstraction and formation of the intermediate with a radical residue in dehydrogenation/hydroxylation reactions, and the formation of a C–O bond to form the radical intermediate in epoxidation reactions, respectively (see Schemes 3, 4). Therefore, we can directly compare the activation parameters determined for compounds I and II for the particular type of oxygenation reactions, as they can be associated with the same rate-limiting steps.

Upon injection of a substrate into the reaction mixture, the decomposition reaction of the generated intermediate was observed, which is directly related to the reaction with the substrate. In all cases the reactive intermediates reverted to iron(III) porphyrin species, giving clean isosbestic points in the resulting rapid-scan spectra recorded during the overall reaction sequence (see Figs. 2, 3, S3–S5). In all reactions compound I or compound II was remarkably stable even at high temperatures, and the spontaneous decomposition of these reactive intermediates was extremely slow compared with the observed reaction with the substrate (see Fig. S6). Moreover, the single-exponential fits of the kinetic traces obtained indicate that only primary oxidation reactions have to be taken into account since secondary reactions are not involved.

Two reaction steps operate in the hydroxylation or dehydrogenation reactions of compound I, viz., an initial reduction of the cation radical species [$(TMP^{\cdot+})Fe^{IV}$=O] to [$(TMP)Fe^{IV}$–OH], which can also be regarded as a compound II intermediate [57–59], and a second, very fast "rebound" step ending with the reformation of an iron(III) porphyrin (see Fig. S3) [10, 41, 43]. Since the lifetimes of the radical intermediates are known to be ultrashort because the rebound step is extremely fast [2, 4, 10], only the rate-determining initial step is reflected in the k_{obs} values determined. In contrast, in the case of C–H abstraction reactions with compound II, a single reaction step operates, which is also equivalent to C–H abstraction (see Figs. 2, 3). Therefore, this C–H abstraction step can be

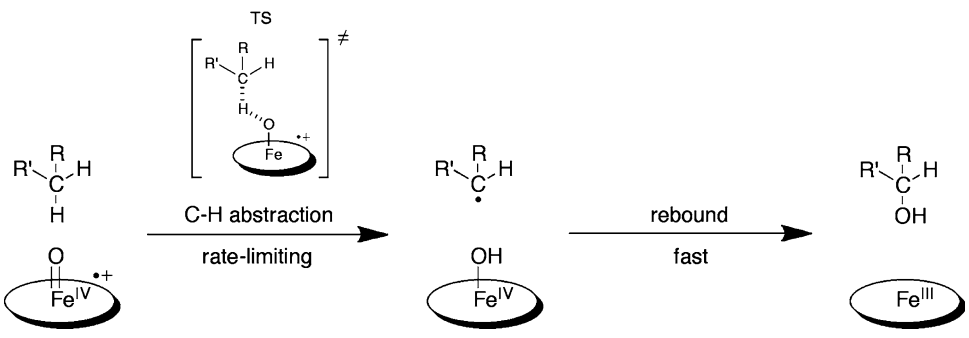

Scheme 3 The "rebound mechanism" in hydroxylation reactions with compound I including the transition state (*TS*) for the rate-limiting step [5, 10]

Scheme 4 The mechanism for epoxidation reactions with compound I including the transition state (*TS*) for the rate-limiting step [10]

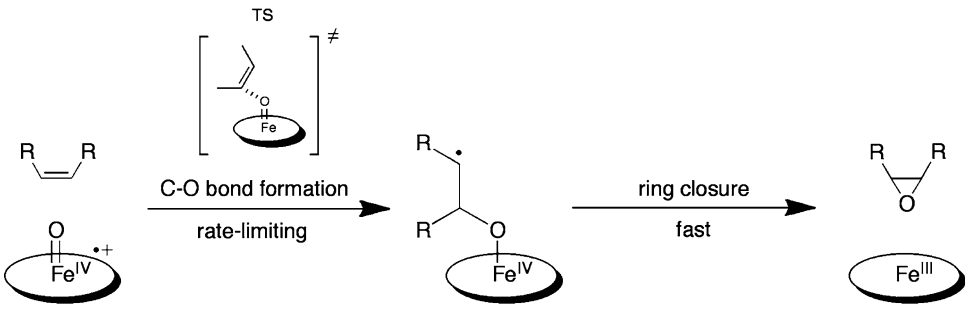

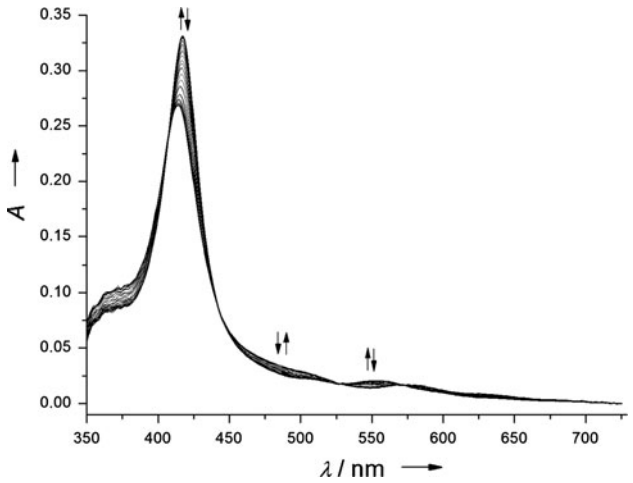

Fig. 2 Rapid-scan spectra for the conversion of [Fe^{III}(TMP)OH] into compound II upon addition of iodosylbenzene (PhIO) with the subsequent reformation of [Fe^{III}(TMP)OH] upon addition of xanthene. Experimental conditions: 2.7×10^{-6} M Fe^{III}(TMP)OH, 6.0×10^{-6} M PhIO, 4.5×10^{-3} M xanthene in acetonitrile at − 15 °C

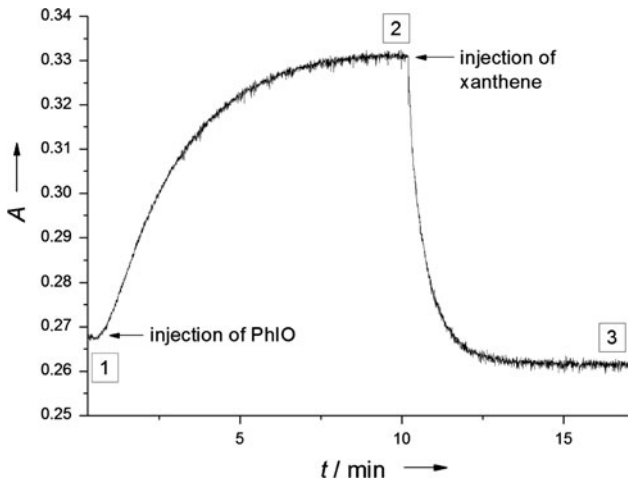

Fig. 3 Kinetic trace for the reaction shown in Fig. 2 recorded at the Soret band (417 nm). Starting with [Fe^{III}(TMP)OH] (*1*), the addition of PhIO leads to the formation of compound II (*2*). Upon addition of xanthene, the reduction back to [Fe^{III}(TMP)OH] (*3*) can be monitored. Experimental conditions: 2.7×10^{-6} M Fe^{III}(TMP)OH, 6.0×10^{-6} M PhIO, 4.5×10^{-3} M xanthene in acetonitrile at –15 °C

investigated for the reaction of DHA or xanthene with each of the two reactive intermediates. In the same manner, this can also be accomplished for the rate-determining C–O bond formation step in epoxidation reactions (see Figs. S4, S5).

For both oxidizing species, k_{obs} showed a linear dependence on the substrate concentration with no significant intercept even at higher temperatures (see Fig. S7). This finding unambiguously rules out the participation of side reactions such as competing spontaneous decomposition of the reactive intermediate, the reformation of the latter with an excess of oxidant present in the reaction medium, and the contribution of secondary oxidations of the substrate in the measured processes.

To ensure that the reformation of compound I or compound II is not reflected in the resulting rate constants, the observed rate constants for the formation of the oxidizing species and for its decomposition in the reaction with the substrate were tuned in such way (based on the known second-order rate constants for these reactions and the relative concentration of the substrate and oxidant used) that the reformation of the respective intermediate did not have a notable effect on the resulting data.

To compare the particular reactivity of each oxidizing intermediate at different temperatures (usually between −25 and 5 °C), we examined their reactions with various substrates under pseudo-first-order conditions. As demonstrated by Fig. 4, the reaction rate shows a significant dependence on the selected temperature (see also Figs. S8–S10). According to the logarithmic form of the Eyring equation, the enthalpy of activation can be calculated from the slope and the entropy of activation can be calculated from the intercept of the resulting linear plot of $\ln(k^{\text{compound I}}/T)$ versus $1/T$ or $\ln(k^{\text{compound II}}/T)$ versus $1/T$ for the oxygenation reactions by compounds I and II, respectively (see Figs. 5, 6). A summary of the activation parameters determined is presented in Table 1.

The second-order rate constants at −15 °C (see Table 1) calculated from the activation parameters are in close agreement with those determined from the concentration dependence measurements in our earlier study [36], which

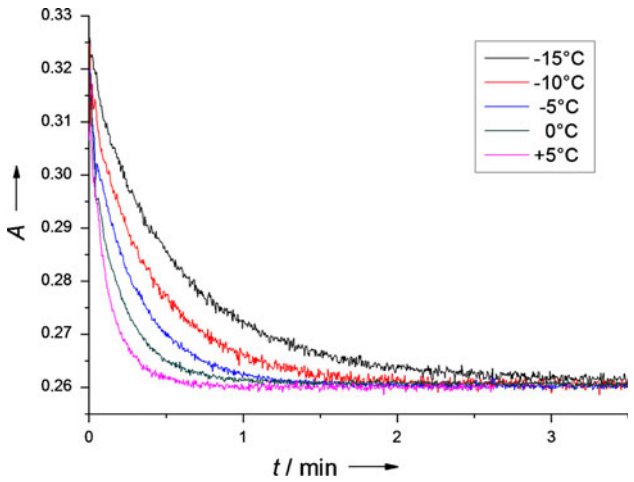

Fig. 4 The temperature-dependent reduction of compound II back to [Fe^{III}(TMP)OH] can be monitored upon addition of xanthene. Experimental conditions: 2.7 × 10^{-6} M Fe^{III}(TMP)OH, 6.0 × 10^{-6} M PhIO, 4.5 × 10^{-3} M xanthene in acetonitrile. Kinetic traces recorded at the Soret band (417 nm)

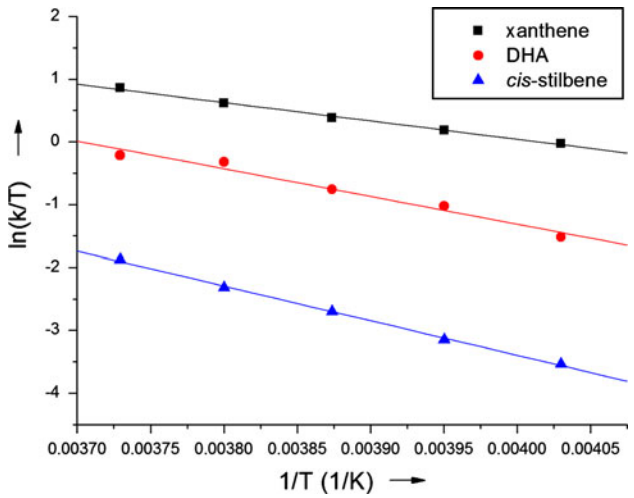

Fig. 5 Determination of the thermal activation parameters by temperature-dependent measurements of the reaction of compound I with various substrates

further supports the proposal that the resulting activation parameters can be assigned to the reactions investigated.

Discussion

The results summarized in Table 1 allow us to distinguish between contributions arising from the activation enthalpy ($\Delta H^{\neq}$) and the activation entropy (expressed as $T\Delta S^{\neq}$) towards the overall activation barrier ($\Delta G^{\neq} = \Delta H^{\neq} - T\Delta S^{\neq}$). In this way it is possible to draw conclusions concerning the importance of enthalpy and entropy effects during the oxygenation of different substrates by the model

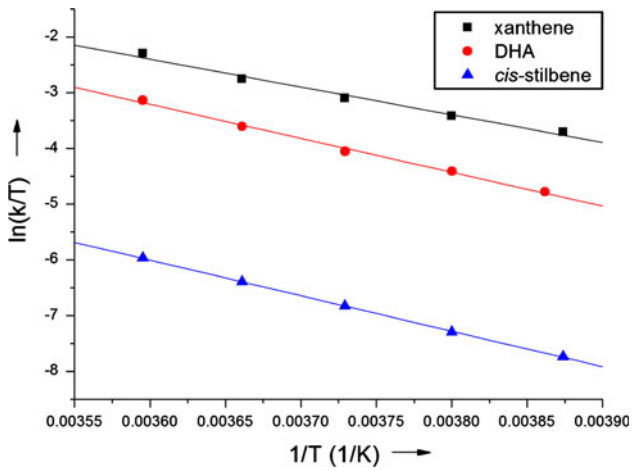

Fig. 6 Determination of the thermal activation parameters by temperature-dependent measurements of the reaction of compound II with various substrates

complexes for compounds I and II. For most of the reactions studied, the activation enthalpy contributes most to the overall activation barrier. Only in a few cases does the activation entropy make a considerable contribution or contribute even more than the activation enthalpy. These general trends form the basis for the further discussion.

If C–H abstraction reactions are enthalpy-controlled, the respective rate constants should be closely related to the strength of the bond to be activated. Since the formation of the transition state is connected with partial electron transfer from the carbon atom, accompanied by the partial dissociation of the C–H bond with a concomitant formation of an O–H bond, it can be expected that the activation barriers for the formation of the transition state should correlate with the dissociation energies of C–H and O–H bonds, i.e., BDE_{C-H} and BDE_{O-H}, respectively. If we consider substrate oxygenation reactions by one oxidant (compound I or compound II), the BDE_{O-H} value remains constant throughout the series of hydrogen abstraction reactions with various substrates. Therefore, only the correlation of the activation barrier, $\Delta H^{\neq}$, with BDE_{C-H} has to be considered. As a result, this bond strength should be reflected by the activation enthalpy, i.e., a stronger C–H bond requires a higher activation enthalpy, which causes a higher activation barrier ($\Delta G^{\neq}$) and consequently a lower rate constant for this particular reaction. This trend can be observed when comparing the activation parameters determined for DHA and xanthene (i.e., a lower BDE_{C-H} causes a lower $\Delta H^{\neq}$, which leads to a lower $\Delta G^{\neq}$ and a higher rate constant).

Comparison of the activation enthalpies for compound I with those for compound II measured for the same substrate reveals that the activation enthalpies for the reaction of compound I are substantially lower than those for

Table 1 Activation parameters, C–H bond energies [70], and rate constants calculated from $\Delta G^{\neq}$ at −15 °C for the reaction of compounds I and II with various substrates

Substrate	$\Delta H^{\neq}$ (kJ/mol)	$\Delta S^{\neq}$ (J/K mol)	$-T_{-15\ ^\circ C}\Delta S^{\neq}$ (kJ/mol)	$\Delta G^{\neq}_{-15^\circ C}$(kJ/mol)	BDE_{C-H} (kJ/mol)	$k^{CpdI(-15^\circ C)}$ $[M^{-1}\ S^{-1}]$
Compound I						
cis-Stilbene	46 ± 1	−43 ± 4	11 ± 1	57 ± 2	–	15.8 ± 0.6
DHA	42 ± 1	−41 ± 5	11 ± 1	53 ± 2	319.45	(1.01 ± 0.04) × 10^2
Xanthene	24.4 ± 0.9	−100 ± 4	25 ± 1	49 ± 5	310.66	(6.5 ± 0.7) × 10^2
Compound II						
cis-Stilbene	52.9 ± 0.5	−57 ± 2	14.7 ± 0.5	68 ± 1	–	0.094 ± 0.001
DHA	51 ± 3	−41 ± 5	11 ± 2	62 ± 5	319.45	1.5 ± 0.1
Xanthene	37 ± 1	−85 ± 5	22 ± 2	59 ± 3	310.66	6.2 ± 0.3

DHA 9,10-dihydroanthracene, *BDE* bond dissociation energy

compound II. This finding is in agreement with the experimentally observed oxygenation strength of these two oxidants. Significantly higher activation barriers for compound II indicate that the hydrogen abstraction by compound II is sluggish compared with that for compound I. Theoretical calculations of activation barriers, viz., quantum mechanical/molecular mechanical studies, demonstrated that hydrogen abstraction barriers for compound II are approximately 16 kJ/mol higher than those for compound I [60, 61]. In this work we found the experimentally determined differences between the activation enthalpies for compounds I and II measured for various substrates to range between 9 and 13 kJ/mol depending on the substrate used.

It seems that the low barrier for C–H activation for xanthene is the result of other factors. According to the computational calculations, the barrier for the C–H abstraction reaction can be lowered by an increase in resonance energy of the transition state. It can be expected that in the case of xanthene an increase in resonance energy caused by an enhanced conjugation of the oxygen lone pair results in a decrease of the activation barrier [62]. In the same way, the activation entropy is also affected, since this stabilization suggests energetically more stable intermediates and thus a closer interaction between the reaction partners. Consequently, their translational and rotational degrees of freedom are limited, which is reflected by a more negative $\Delta S^{\neq}$ compared with that for DHA.

Although the bond energies can be regarded as the thermodynamic driving force, they do not necessarily correlate with the level of the activation barrier for the transition state. According to recent findings from computational studies [62], the calculated activation barriers can show a poor correlation with BDE_{C-H}, but a very good correlation with the bond strength quantity (D_{C-H}). The latter is a more reliable measure of the interaction strength between the bound alkane and hydrogen moieties, and is defined as the combination of BDE_{C-H} and the energy difference of the alkyl residue in the free substrate and in the fully relaxed geometry of the alkyl radical (RE_{Alk}), i.e., $D_{C-H} = BDE_{C-H} + RE_{Alk}$. Consistent with this finding is the possibility that the substrates characterized by higher BDE_{C-H} can display a similar or even lower energy barrier for the transition state than a substrate with lower BDE_{C-H} if the value of RE_{Alk} is high enough. This is the case when the formation of the alkyl radical residue in the transition state is energetically favorable. When we take into account that the RE_{Alk} values for the substrates studied can differ (especially in the case of xanthene, owing to the stabilizing resonance energy), the combination of a low activation enthalpy with a relatively high BDE_{C-H} observed in our study appears to be reasonable and in line with computational predictions.

Moreover, $\Delta H^{\neq}$ might not even play a decisive role for the height of the activation barrier and thus for the resulting rate constants. In the case of DHA, the overall process is clearly enthalpy-controlled, whereas for xanthene the activation entropy also contributes significantly, especially in the case of compound I, where the contribution of $T\Delta S^{\neq}$ is very similar to that of $\Delta H^{\neq}$.

As mentioned before, hydroxylation reactions follow the oxygen rebound mechanism that involves a rate-determining C-H abstraction as the first reaction step [10, 41, 54, 55]. Takahashi et al. [43] found that this type of reaction can be entropy-controlled when the cation radical compound I is used as oxidizing species. This finding implies that the initial hydrogen abstraction step requires a highly ordered transition state characterized by a loss of translational and rotational degrees of freedom that results in a significantly negative $\Delta S^{\neq}$. On the basis of the data given in Table 1, one can calculate that in the reaction of xanthene with compound I the entropy term $T\Delta S^{\neq}$ shows a higher contribution than $\Delta H^{\neq}$ to $\Delta G^{\neq}$ at temperatures above −29.2 °C. In contrast, the reactions with DHA show a significantly less negative activation entropy and are therefore enthalpy-controlled. To understand this

difference, one should consider that DHA is a symmetrical molecule, whereas xanthene has a notable dipole moment that originates from the partially negatively charged oxygen bridge and a more positive CH_2 bridge on the opposite side of the molecule [63]. If we consider that both reactive intermediates (compounds I and II) bear a very positive iron center, a possible explanation is that xanthene tends to approach the reaction partner in a "wrong" orientation in contrast to DHA, i.e., with the oxygen bridge pointing to the iron center. If we keep in mind that compound II is an iron(IV) species, whereas compound I is an iron(IV) cation radical [and therefore a formal iron(V) species], it is reasonable that this effect might have a larger impact on reactions with compound I owing to its higher charge, which is in line with the data given in Table 1.

In contrast, the reaction with the symmetrical DHA molecule shows no difference in the activation entropies and gives almost identical values for the reaction with compounds I and II. In this case the difference in the reactivity clearly arises from different activation enthalpies, which reflect a higher ability of compound I to induce C–H abstraction processes. For this reason, the reaction with DHA is enthalpy-controlled, no matter whether the reaction partner is compound I or compound II. In contrast, the corresponding reaction of xanthene with the cation radical species (compound I) is entropy-controlled, whereas the reaction with compound II is still enthalpy-controlled as here the activation enthalpy is generally higher.

To further clarify this impact, we studied another common type of reaction, viz., the epoxidation of *cis*-stilbene. In this case we are dealing with a partially negatively charged double bond, and it is therefore likely that its attraction to a more positively charged iron center bearing a more electrophilic oxygen promotes the reaction with compound I more than the reaction with compound II, since different contributions from aspects such as orientation, trajectory, and accessibility can be expected. Consequently, $\Delta S^{\neq}$ is less negative for compound I than for compound II in epoxidation reactions, whereas the opposite effect is observed when C–H abstraction reactions are studied.

In summary, the differences in the activation enthalpies can largely account for the higher reactivity of compound I compared with compound II in epoxidation as well as in C–H abstraction reactions. This result reflects the higher oxidative power of compound I and is in line with a stronger Fe=O bond and stronger stabilization of oxygen in compound II models as reported in the literature [64]. This effect might be smaller than expected since similar bond lengths were found for the Fe=O moiety in some compound I and compound II species [65].

The epoxidation reaction is clearly enthalpy-controlled for both compound I and compound II models, which is in agreement with the results from previous studies on compound I mimics [43]. As a consequence, the difference in the reactivity between compounds I and II for the epoxidation of *cis*-stilbene clearly arises from effects that control the activation enthalpy, i.e., factors such as bond strength rather than the order of the transition state. This is in sharp contrast to the results for C–H abstraction reactions, where different entropic factors induce different reactivities for compounds I and II, as this reaction proceeds via another pathway and transition state.

The large impact of the activation entropy, in general, and the entropic control of the hydrogen abstraction reaction of xanthene with compound I, in particular, have important consequences for practical work as well as for theoretical considerations. For such a scenario the Gibbs free energy relationship $\Delta G^{\neq} = \Delta H^{\neq} - T\Delta S^{\neq}$ demands a close relation with the reaction temperature. As shown in Table 1, at −15 °C the reaction of compound I with DHA has a contribution from the activation entropy of 11 kJ/mol to the overall activation barrier of $\Delta G^{\neq}_{-15^{\circ}\mathrm{C}} = 53\,\mathrm{kJ/mol}$, whereas the reaction of xanthene has a much larger entropy contribution of $-T\Delta S^{\neq} = 25.7$ kJ/mol and $\Delta H^{\neq} = 24.4$ kJ/mol to the free energy activation barrier. Consequently, the reaction of compound I with xanthene becomes slower compared with the reaction with DHA on increasing the temperature. On the basis of the data given, an isokinetic temperature of 25.2 °C can be calculated where both reactions have the same activation barrier. Upon a further increase in temperature, the reaction rate for the C–H abstraction of compound I with DHA even exceeds that for the reaction with xanthene. Even though the respective reactions with compound II are in general enthalpy-controlled, the isokinetic temperature describing this change in the reactivity order is only 45.0 °C, as in the case of xanthene again a lower activation enthalpy is combined with an about twice as high activation entropy in comparison with DHA (see the example in Table 1 at −15 °C). Although the isokinetic temperatures given should be evaluated with caution since they include large error limits due to the calculation method, they at least suggest that these switchover points can play a role in a biologically relevant temperature range.

In the same way, a change in regioselectivity by the variation of the temperature in the competitive C=C bond epoxidation versus C–H hydroxylation of cyclohexene has been reported in some cases [42]. Again, this can be accounted for in terms of a large contribution of the activation entropy term to the activation barrier in hydroxylation reactions that increases with temperature, whereas the epoxidation reaction is clearly dominated by the activation enthalpy. Therefore, the latter becomes favorable over the hydroxylation reaction at higher temperatures.

In this respect, also some theoretical approaches that are based on the application of the activation energy E_a should be reconsidered, since E_a neither reflects entropic effects nor shows a dependence on the temperature. As a consequence, the use of E_a instead of $\Delta G^{\neq}$ in computational studies can be misleading when the activation entropy (and in this respect also the temperature) plays a dominant role [43].

Furthermore, a common method to visualize a direct relationship between the C–H bond strength and the rate constants for the rate-determining hydrogen abstraction reaction is to plot $\log(k/n)$ versus BDE_{C-H} (where n is the number of abstractable substrate hydrogen atoms). This plot is expected to result in a linear relationship showing that $\log(k/n)$ decreases with increasing bond strength according to the Bell–Evans–Polanyi relationship [66, 67]. Remarkably, such a close connection between BDE_{C-H} and $\Delta H^{\neq}$ is not necessarily given, as discussed above. In addition, this correlation demands enthalpy-controlled reactions, as only in that case can bond strengths be liable for the resulting rate constants by affecting the dominant activation enthalpy and in this way the activation barrier. As soon as the activation entropy plays a major role in the activation process, such a close relation no longer exists, although the logarithmic expression of the rate constants as well as compensation effects might cover the decreasing impact of the bond strength if the data set is limited to only a few substrates. Nevertheless, especially weak C–H bonds suggest a relatively large influence of the activation entropy. Consequently, a plot of the low BDE values versus $\log(k/n)$ should result in a horizontal line. This fact has been intensively discussed for different hydrogen-abstracting agents such as the *t*-butoxyl radical [68], but has been widely ignored when considering reactions of P450 biomimetics.

Transferring the results of biomimetic studies at low temperatures to biological conditions even amplifies the relevance of the entropic contribution. Furthermore, enzymes appear to have sterically more demanding superstructures. On the other hand, the entropic impact may be compensated by the fact that water molecules leave the active pocket when substrates enter. Therefore, these molecules already lose a large part of their rotational and translational degrees of freedom prior to the actual reaction with the iron center. As a consequence, the activation entropy, and for this reason the free energy barrier, for enzyme reactions is usually lower than for bimolecular model system reactions [5, 69].

Conclusion

In conclusion, we performed the first comparative study to evaluate thermal activation parameters for biomimetic models for compounds I and II in epoxidation and C–H abstraction reactions. This comparison reveals an important impact of the chemical nature of the substrate and the reactive intermediate (viz., compound I or compound II) on the resulting reaction rate in different types of reaction, which goes beyond the common concepts that relate the activation barrier to bond energies in C–H abstraction reactions. In fact, the crucial question is to what extent the activation entropy contributes to the overall activation barrier and thus to the resulting rate constants.

As demonstrated in this study, epoxidation reactions are clearly enthalpy-controlled, whereas C–H abstraction reactions can in many cases be dominated by factors contributing to the activation entropy. Since an important impact of the activation entropy contribution leads to a significant dependence of the activation barrier on the temperature, a close correlation between bond strength and reaction rate—as commonly assumed for C–H abstraction reactions—no longer exists. In this respect, also theoretical calculations using the activation energy (E_a) instead of $\Delta G^{\neq}$ as a measure for the activation barrier have to be interpreted with caution, because E_a is independent of temperature.

Therefore, comparative studies in which rate constants for different substrates, different reaction types, or different reactive intermediates (viz., compounds I and II) are determined can in some cases be misleading. As a consequence, the particular impact of the entropic contribution and a possible influence of the reaction temperature should be considered when evaluating experimental as well as theoretical results, as these effects can cause substantial changes in the reactivity order of different catalytic species.

Acknowledgment The authors gratefully acknowledge continued financial support from the Deutsche Forschungsgemeinschaft.

References

1. Denisov IG, Makris TM, Sligar SG, Schlichting I (2005) Chem Rev 105:2253–2277
2. Meunier B, de Visser SP, Shaik S (2004) Chem Rev 104:3947–3980
3. Shaik S, Kumar D, de Visser SP, Altun A, Thiel W (2005) Chem Rev 105:2279–2328
4. Shaik S, Cohen S, Wang Y, Chen H, Kumar D, Thiel W (2010) Chem Rev 110:949–1017
5. Shaik S, Hirao H, Kumar D (2007) Nat Prod Rep 24:533–552
6. Li C, Zhang L, Zhang C, Hirao H, Wu W, Shaik S (2007) Angew Chem 119:8316–8318
7. Park MJ, Lee J, Suh Y, Kim J, Nam W (2006) J Am Chem Soc 128:2630–2634
8. Seo MS, Kamachi T, Kouno T, Murata K, Park MJ, Yoshizawa K, Nam W (2007) Angew Chem 119:2341–2344

9. Shaik S, Cohen S, de Visser SP, Sharma PK, Kumar D, Kozuch S, Ogliaro F, Danovich D (2004) Eur J Inorg Chem 2:207–226
10. Shaik S, de Visser SP, Ogliaro F, Schwarz H, Schröder D (2002) Curr Opin Chem Biol 6:556–567
11. Schröder D, Shaik S, Schwarz H (2000) Acc Chem Res 33:139–145
12. Ogliaro F, de Visser SP, Cohen S, Sharma PK, Shaik S (2002) J Am Chem Soc 124:2806–2817
13. Sharma PK, de Visser SP, Shaik S (2003) J Am Chem Soc 125:8698–8699
14. Schöneboom JC, Cohen S, Lin H, Shaik S, Thiel W (2004) J Am Chem Soc 126:4017–4034
15. Eda M, Kamachi T, Yoshizawa K, Toraya T (2002) Bull Chem Soc Jpn 75:1469–1481
16. Shaik S, Hirao H, Kumar D (2007) Acc Chem Res 40:532–542
17. Cryle MJ, De Voss JJ (2006) Angew Chem 118:8401–8403
18. Cryle MJ, De Voss JJ (2006) Angew Chem Int Ed 45:8221–8223
19. de Ortiz Montellano PR, De Voss JJ (2002) Nat Prod Rep 19:477–493
20. Franke A, Fertinger C, van Eldik R (2008) Angew Chem Int Ed 47:5238–5242
21. Nam W, Ryu YO, Song WJ (2004) J Biol Inorg Chem 9:654–660
22. Nam W, Lim MH, Lee HJ, Kim C (2000) J Am Chem Soc 122:6641–6647
23. Collman JP, Chien AS, Eberspacher TA, Brauman JI (2000) J Am Chem Soc 122:11098–11100
24. Collman JP, Zeng L, Decrèau RA (2003) Chem Commun 2974–2975
25. Machii K, Watanabe Y, Morishima I (1995) J Am Chem Soc 117:6691–6697
26. Nam W, Jin SW, Lim MH, Ryu JY, Kim C (2002) Inorg Chem 41:3647–3652
27. Jin S, Bryson TA, Dawson JH (2004) J Biol Inorg Chem 9:644–653
28. Vaz ADN, McGinnity DF, Coon MJ (1998) Proc Natl Acad Sci USA 95:3555–3560
29. Vaz ADN, Pernecky SJ, Raner GM, Coon MJ (1996) Proc Natl Acad Sci USA 93:4644–4648
30. Newcomb M, Hollenberg PF, Coon MJ (2003) Arch Biochem Biophys 409:72–79
31. Nam W, Lim MH, Moon SK, Kim C (2000) J Am Chem Soc 122:10805–10809
32. Adam W, Roschmann KJ, Saha-Möller CR, Seebach D (2002) J Am Chem Soc 124:5068–5073
33. Kang Y, Chen H, Jeong YJ, Lai W, Bae EH, Shaik S, Nam W (2009) Chem Eur J 15:10039–10046
34. Takahashi A, Kurahashi T, Fujii H (2009) Inorg Chem 48:2614–2625
35. Collman JP, Zeng L, Brauman JI (2004) Inorg Chem 43:2672–2679
36. Fertinger C, Hessenauer-Ilicheva N, Franke A, van Eldik R (2009) Chem Eur J 15:13435–13440
37. Fujii H, Kurahashi T, Tosha T, Yoshimura T, Kitagawa TJ (2006) Inorg Biochem 100:533–541
38. Dolphin D, Traylor TG, Xie LY (1997) Acc Chem Res 30:251–259
39. Nam W (2007) Acc Chem Res 40:522–531
40. Traylor TG, Kim C, Richards JL, Xu F, Perrin CL (1995) J Am Chem Soc 117:3468–3474
41. Kumar D, Tahsini L, de Visser SP, Kang HY, Kim SJ, Nam W (2009) J Phys Chem A 113:11713–11722
42. Song WJ, Ryu YO, Song R, Nam W (2005) J Biol Inorg Chem 10:294–304
43. Takahashi A, Kurahashi T, Fujii H (2007) Inorg Chem 46:6227–6229
44. Cheng RJ, Latos-Grazynski L, Balch AL (1982) Inorg Chem 21:2412–2418
45. Saltzmann H, Sharefkin JG (1963) Org Synth 43:60–61
46. Groves JT, Watanabe Y (1986) J Am Chem Soc 108:7834–7836
47. Groves JT, Watanabe Y (1988) J Am Chem Soc 110:8443–8452
48. Wolak M, van Eldik R (2007) Chem Eur J 13:4873–4883
49. Nam W, Lim MH, Oh SY (2000) Inorg Chem 39:5572–5575
50. Pan Z, Newcomb M (2007) Inorg Chem 46:6767–6774
51. Groves JT, Gross Z, Stern MK (1994) Inorg Chem 33:5065–5072
52. Nam W, Park SE, Lim IK, Lim MH, Hong J, Kim J (2003) Am Chem Soc 125:14674–14675
53. Jeong YL, Kang Y, Han AR, Lee YM, Kotani H, Fukuzumi S, Nam W (2008) Angew Chem Int Ed 47:7321–7324
54. Groves JT, McClusky GA, White RE, Coon MJ (1978) Biochem Biophys Res Commun 81:154–160
55. Rittle J, Green MT (2010) Science 330:933–937
56. Van Rantwijk F, Sheldon RA (2000) Curr Opin Biotechnol 11:554–564
57. Stephenson NA, Bell AT (2007) J Mol Catal A 275:54–62
58. Stone KL, Behan RK, Green MT (2006) Proc Natl Acad Sci USA 103:12307–12310
59. Hersleth HP, Uchida T, Røhr AK, Teschner T, Schünemann V, Kitagawa T, Trautwein AX, Görbitz CH, Andersson KK (2007) J Biol Chem 32:23372–23386
60. Altun A, Shaik S, Thiel W (2007) J Am Chem Soc 129:8978–8987
61. Tahsini L, Bagherzadeh M, Nam W, de Visser SP (2009) Inorg Chem 48:6661–6669
62. Shaik S, Kumar D, de Visser SP (2008) J Am Chem Soc 130:10128–10140
63. Schaefer T, Sebastian R (1990) Can J Chem 68:1548–1552
64. Sugimoto H, Tung HC, Sawyer DT (1988) J Am Chem Soc 110:2465–2470
65. Newcomb M, Halgrimson JA, Horner JH, Wasinger EC, Chem LX, Sligar SG (2008) Proc Natl Acad Sci USA 105:8179–8184
66. Bell RP (1936) Proc R Soc London Ser A 154:414–421
67. Evans MG, Polanyi M (1938) Trans Faraday Soc 34:11–24
68. Finn M, Friedline R, Suleman NK, Wohl JC, Tanko JM (2004) J Am Chem Soc 126:7578–7584
69. Page MI, Jencks WP (1971) Proc Natl Acad Sci USA 68:1678–1683
70. Stein SE, Brown RL (1991) J Am Chem Soc 113:787–793